Published in final edited form as:
Nat Chem. 2010 December ; 2(12): 1025–1030. doi:10.1038/nchem.871.

Storable, thermally activated, near-infrared chemiluminescent dyes and dye-stained microparticles for optical imaging

Jeffrey M. Baumes, **Jeremiah J. Gassensmith**, **Jay Giblin**, **Jung-Jae Lee**, **Alexander G. White**, **William J. Culligan**, **W. Matthew Leevy**, **Masaru Kuno**, and **Bradley D. Smith***
Department of Chemistry and Biochemistry, 236 Nieuwland Science Hall, University of Notre Dame, Notre Dame, IN 46556, USA

Abstract

Optical molecular imaging employs relatively harmless, low-energy light and technically straightforward instrumentation. Self-illuminating, chemiluminescent systems are especially attractive since they have inherently high signal contrast due to the lack of background emission. Currently, chemiluminescence imaging involves short-lived molecular species that are not stored but instead generated *in situ*, and they typically emit visible light, which does not penetrate far through heterogeneous biological media. Here, we describe a new paradigm for optical molecular imaging using squaraine rotaxane endoperoxides (SREPs), interlocked fluorescent and chemiluminescent dye molecules that have a squaraine chromophore encapsulated inside a macrocycle endoperoxide. SREPs can be stored indefinitely at temperatures below −20 °C, but upon warming to body temperature they undergo a unimolecular chemical reaction and emit near infrared light that can pass through a living mouse. Dye-stained microparticles are easily prepared for *in vivo* near-infrared optical imaging using commercial imaging stations.

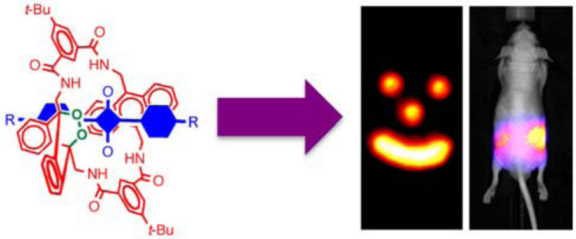

Radiotracers are molecular probes containing radioactive isotopes whose high-energy emission can be detected at extremely low concentrations.[1] The radioisotopes are typically generated and detected using sophisticated equipment and some radioisotopes, especially positron emitters, decay rapidly thus limiting their shelf life. High-energy radiation readily passes through tissue which is valuable for medical imaging; however, the radiation can also induce ionization processes that are potentially harmful to living systems.[2] Indeed, the

*smith.115@nd.edu.

See the Supplementary Information for complete listing of spectral data, structure elucidation, kinetic analyses, control experiments, and image analyses.

Author contributions

B.D.S conceived this project and J.M.B. helped design the experiments. J.J.G., J-J.L., W.J.C., A.G.W., W.M.L., J.G. and M.K. contributed to the experimental work and data analysis. B.D.S and J.M.B. wrote the paper, and all co-authors contributed comments.

Additional information

The authors declare no competing financial interests. Supplementary information accompany this paper at www.nature.com/naturechemistry. Reprints and permission information is available online at http://npg.nature.com/reprintsandpermissions.

targeted delivery of cytotoxic radiation to sites of disease is the cornerstone of radioimmunotherapy.[3] Chemiluminescent molecules are conceptually similar to radiotracers, but with several notable differences.[4] They are typically unstable, transient species that are generated by stoichiometric or enzymatic oxidation reactions.[5] Most chemiluminescent compounds emit visible light, which is relatively harmless and easily detected, but it is readily absorbed and scattered by biological matrices.[6, 7] These factors combine to limit the utility of chemiluminescence for *in vivo* molecular imaging of tissue and living animals.

Here we describe the first example of a new family of highly fluorescent and chemiluminescent compounds called squaraine rotaxane endoperoxides (SREPs) and we show why they may be suitable for many types of molecular imaging and biotechnology applications. The lead structure is **1EP**, a permanently interlocked [2] rotaxane comprised of a dumb-bell shaped squaraine dye encapsulated by a tetralactam macrocycle that contains a thermally unstable 9,10-anthracene endoperoxide group (Fig. la).8 The cycloreversion reactions of aromatic endoperoxides are known to exhibit chemiluminescence.[9] As [2]rotaxanes, SREPs are well suited for programmable chemiluminescence because the surrounding macrocycle endoperoxide acts as an energy source for the mechanically bonded squaraine chromophore whose excited singlet state emits light with high efficiency. We report that prototype **1EP** is easily generated by simply irradiating the parent squaraine rotaxane **1** with red light in the presence of air, and that it can be stored indefinitely at −20 °C until needed. Upon warming to body temperature, **1EP** undergoes a unimolecular cycloreversion reaction that releases singlet oxygen and emits near-infrared light that can pass through a living mouse. The chemiluminescent signal is detected with inherently high contrast because there is negligible background emission from the animal.

Results and discussion

The permanent encapsulation of squaraine **3** inside macrocycle **2** to make squaraine rotaxane **1** is achieved in high yield and large scale using straightforward synthetic methods.[10] Squaraine rotaxanes strongly absorb deep-red light and they are weak to moderate photosensitizers of molecular oxygen.[11, 12] Therefore, it is not surprising that irradiation of **1** with red light in the presence of air results in a 9,10-anthracene endoperoxide product. However, the highly selective formation of mono(endoperoxide) **1EP** is noteworthy because it contrasts with the known reactivity of the free parent macrocycle **2** where both anthracene units are attacked by singlet oxygen.[13] Apparently, the encapsulated squaraine prevents cycloaddition to the second anthracene unit in **1EP.** The formation of **1EP** is extremely clean (Fig. lb); extended irradiation does not lead to any additional photochemical reaction and no chemical change occurs if air is excluded from the irradiated sample. The molecular formula and molecular connectivity of **1EP** were readily assigned by mass spectral and multidimensional NMR methods (see Supplementary Information online). Proof that the endoperoxide group is located inside the macrocycle (internal stereoisomer) was gained using variable temperature ^{1}H NMR spectroscopy (see Supplementary Fig. S7 online).

Typically, 9,10-dialkylanthracene endoperoxides undergo skeletal rearrangements rather than cycloreversion reactions.[14] In notable contrast, endoperoxide **1EP** cycloreverts at room temperature to completely regenerate the starting squaraine rotaxane and release molecular oxygen (see Supplementary Figs. S9–S11 online). The rate constant for cycloreversion was determined by monitoring restoration of the anthracene absorption band centered at 372 nm. In *o*-xylene solvent at 38 °C, the first order rate constant was 8.7×10^{-2} h^{-1}, which corresponds to a half-life of 8 hours. Essentially the same rate constant was obtained when the solvent was changed to the more polar acetonitrile:water, 9:1. An attractive feature with SREPs is the ability to store them at low temperature for extended periods. For example, the activation energy for **1EP** cycloreversion is 88 kJ/mol, and there is no measurable reaction

when samples are maintained below −20 °C. Another defining property of the endoperoxide cycloreversion process is the fraction of molecular oxygen that is released as excited state singlet oxygen. While the decay of singlet oxygen ($^1\Delta$) to triplet ground state ($^3\Sigma$) can be detected directly as weak monomol ($^1O_2$) luminescence at 1270 nm or dimol ($2\bullet^1O_2$) emission at 633 and 703 nm,[9] it was more convenient to conduct singlet oxygen trapping experiments.[15] A number of chemical trapping agents were tested, and the most informative was 2,3-dimethyl-2-butene which reacts with singlet oxygen to give a hydroperoxide product that is readily quantified by ^{1}H NMR spectroscopy.[16] The observed ratio of trapped hydroperoxide to regenerated squaraine rotaxane in $CDCl_3$ indicated that at least 64±10 % of the released molecular oxygen was singlet oxygen (see Supplementary Fig. S12 online).

Shown in Fig. 2a is a false-colored pixel intensity map of the emission from a solution of **1EP** in $CDCl_3$ at 38°C. The chemiluminescence decreases over time but the decay is not a simple exponential, it is a biphasic curve with an initial rapid drop over the first few minutes followed by a slower decay with a half-life of several hours. A concentration study showed that the integrated chemiluminescence intensity for **1EP** was essentially linear over a sixteen-fold concentration range (see Supplementary Fig. S13 online), indicating the potential of SREPs to act as chemiluminescent tags for quantitative detection and sensing. Organic solutions of **1EP** were used to stain hydrophobic surfaces and the cores of polymeric microparticles (Fig. 2b),[17] and chemiluminescence intensity maps of these materials were acquired using a commercial imaging station equipped with a CCD camera. In Fig. 2c is the chemiluminescence from a group of stained, polystyrene particles that are aggregated in a vial containing water, while Fig. 2d depicts an aqueous dispersion of stained polystyrene particles that have been functionalized with carboxylate groups. The potential utility in surface based detection technologies was assessed by spotting samples of **1EP** onto reverse-phase TLC plates (glass sheets supporting a thin layer of porous silica particles with impregnated C18 hydrocarbon). In Figs. 2e–g are bright field, chemiluminescence, and fluorescence images of a surface with a progression of spot sizes. The smallest spot is approximately 1 mm diameter, contains about 17 picomoles of **1EP**, and it is easily identified using either chemiluminescence or fluorescence imaging. This highlights the detection versatility of SREPs. Both **1EP** and the decay product **1** have essentially identical near-infrared fluorescence properties, thus the intrinsic bright fluorescence of a sample spot hardly changes as the chemiluminescence reaction proceeds, which means that the plate can be read by either imaging modality. In this case, the target background ratio (TBR) for fluorescence imaging is ~70 and substantially better than chemiluminescence (TBR = 4.5) because background autofluorescence from the plate is very low and the squaraine chromophore is excited multiple times by the excitation beam.

The chemiluminescence images in Figs. 2a–g were derived from unfiltered photon counts integrated over time, but as illustrated in Fig. 2h the emission is actually localized to the Cy5.5 filter channel (695–770 nm) of the imaging station. Spectral plots of the chemiluminescence and fluorescence emission for **1EP** both exhibit maxima at 733 nm (Fig. 2i), which is significantly different to the maximum expected for singlet oxygen dimol emission (635 and 703 nm). This was confirmed by a control experiment that generated singlet oxygen in the absence of a chromophore and detected its dimol emission in the Ds Red (575–650 nm) channel (see Supplementary Fig. S14 online). Thus, the **1EP** chemiluminescence is emitted from the encapsulated squaraine chromophore whose excited state is activated by the cycloreversion process. The following experiments suggest that chromophore activation is mediated by the released singlet oxygen: (a) The presence of efficient singlet oxygen quenchers, 2,3-dimethyl-2-butene or 1,4-diazabicyclo[2.2.2]octane (DABCO), in solutions of **1EP** greatly diminished the chemiluminescence intensity but had no effect on the fluorescence emission, (b) Chemiluminescence intensity for **1EP** was five

times higher when the solvent was changed from $CHCl_3$ to $CDCl_3$, which correlates with longer singlet oxygen lifetime in the deuterated solvent.[9]

For optical molecular imaging, chemiluminescent probes have a signal contrast advantage over fluorescent probes because there is no excitation beam and thus no background autofluorescence by endogenous biomolecules.[5, 18, 19] However, a drawback with most of the currently available chemiluminescent and bioluminescent systems is they emit visible light, which has poor tissue penetration and large amounts of scattering.[6] The need for next generation systems that emit light within the optimal wavelength window of 650–900 nm is well recognized.[20, 21, 22] The planar optical images in Fig. 3 illustrate the potential value of SREP-labeled microparticles or nanoparticles as chemiluminescent probes for *in vivo* imaging. An aliquot of carboxy functionalized **1EP**-microparticles (50 μL) was injected subcutaneously into the dorsal side of a nude mouse rear leg. In Figs. 3a–c are the high contrast chemiluminescence and reflected fluorescence dorsal images, which required light from the **1EP**-microparticles to pass through ~1 mm of skin. A region of interest (ROI) analysis indicated a TBR of 6.9 for chemiluminescence and 29 for fluorescence (see Supplementary Fig. S15 online). Figs. 3d–f show ventral images which required the light to penetrate a greater thickness of skin and leg tissue (~7 mm). The target signal intensities are attenuated, but the chemiluminescence TBR of 6.8 remains quite good, whereas, the fluorescence TBR of 4.4 is considerably lower. This signal contrast advantage for chemiluminescence increases with tissue penetration distance,[23] as demonstrated by the phantom experiment in Fig. 4. The top row shows that near-infrared chemiluminescence from a small tube containing a solution of **1EP** (250 nmol) passes through a living nude mouse positioned between the tube and the CCD camera. The TBR for the transmitted light is an impressive 11.6, although the image is quite diffuse which is a known characteristic of planar optical imaging, even at near-infrared wavelengths.[24] Signal intensity is strongest at each side of the animal, which coincides with passage through the least amount of tissue. The bottom row in Fig. 4 depicts reflected fluorescence images of the same experimental arrangement; the fluorescence TBR is 1.1 and a comparison of Figs. 4i and 4j shows that fluorescence from the target site (tube containing **1EP**) cannot be readily distinguished from the background produced by scattering of the excitation light and animal autofluorescence. Taken together, the surface and mouse imaging results highlight a potentially attractive feature with SREPs as dual modality molecular imaging probes. They can be used in high contrast chemiluminescence mode to locate relatively deep anatomical locations *in vivo* and subsequently employed in fluorescent mode to identify the microscopic targets within thin histopathology sections taken from the same specimen.

Future efforts to enhance SREP chemiluminescence intensity will undoubtedly be facilitated by a detailed understanding of the chromophore excitation process and its mechanistic relationship with the release of singlet oxygen.[25] Thermally-activated endoperoxide chemiluminescence[26, 27, 28] and the related phenomenon of singlet oxygen sensitized fluorescence[29, 30, 31, 32, 33] have been investigated for more than three decades and the substantial body of published work provides an excellent knowledge base for our ongoing mechanistic studies. It is also worth noting that squaraines are efficient acceptors of singlet oxygen energy.[12] SREPs release singlet oxygen, which is a reactive molecule and one of the primary phototoxic agents in photodynamic therapy. However, singlet oxygen is readily quenched to triplet ground state within a cell, such that the average lifetime is ~3 μs and the diffusion radius only ~100 nm.[34] It is estimated that approximately 10^9 molecules of singlet oxygen are needed to induce a cytotoxic effect[35] which partially explains why most stoichiometric, singlet oxygen release agents exhibit weak biological activity.[36, 37] We have recently reported robust synthetic methods for converting squaraine rotaxanes into fluorescent molecular imaging probes,[8] and it should be quite feasible to incorporate SREPs

within functionalized molecular constructs,[38, 39, 40] or nanoparticles,[41, 42, 43, 44] to make chemiluminescent probes.

Conclusions

Although many organic molecules exhibit chemiluminescence,[4] very few are amenable to synthetic development as storable imaging probes with near-infrared emission. SREPs, as exemplified by lead compound **1EP**, represent a new paradigm for optical molecular imaging. They are easily generated by simple irradiation of the parent squaraine rotaxane with red light in air, and they can be stored and transported at low temperature until needed. Upon warming to body temperature, SREPs emit near-infrared light that can penetrate through a living mouse with high target signal contrast. The chemiluminescent cycloreversion process hardly changes the photophysical properties of the encapsulated squaraine chromophore so a SREP can also be detected using fluorescence, thus providing versatile dual modality optical imaging capability. In many respects, chemiluminescent SREPs are conceptually similar to radiotracers, and they can likely be developed into the chemiluminescent equivalent of radiopharmaceuticals for complementary applications. For example, radiopharmaceuticals are suitable for deep-tissue imaging but they emit ionizing radiation that has an inherent dosimetric health risk.[45] In contrast, chemiluminescent tracers would be restricted to shallower tissues or anatomical sites that can be reached by endoscopes. However, SREPs do not emit harmful radiation, so they may be more appropriate for longitudinal molecular imaging studies that require repeated dosing of the probe, small animal studies that require high throughput, or imaging protocols that gain advantages by employing cheaper, smaller, and safer optical imaging instrumentation. An attractive feature with the modular [2]rotaxane design is that the structural source of the excitation energy (the macrocycle endoperoxide) and the emission chromophore (the encapsulated squaraine) are orthogonal molecular building blocks that are connected by a non-covalent, mechanical bond.[46, 47] They can be modified independently and then interlocked in synthetic combinatorial fashion to create next-generation chemiluminent SREPs with improved performance.

Methods

Synthesis of 1EP

The known rotaxane **1**[10] (15.0 mg, 0.008 mmol) was dissolved in $CDCl_3$ (0.6 mL) and added to a standard NMR tube. The uncapped tube was placed 10 cm in front of a filtered (longpass 520 nm) 150 W Xenon lamp and irradiated for 30 mins with exposure to atmospheric oxygen. Complete conversion to **1EP** was confirmed by ^{1}H NMR spectroscopy. The solvent was removed under reduced pressure at ice bath temperature to give pure **1EP** which was stored as a solid or organic solution at temperatures below −20 °C until needed. Safety note: organic endoperoxides with high oxygen content are potentially shock sensitive materials and should be handled in small portions.

Staining polymeric microparticles and hydrophobic surfaces with 1EP

Polymeric microparticles: An aliquot of THF (160 μL) was added to 2.0 mL aqueous suspension of either 1.0 % (w/v) polystyrene microparticles (5.3 μm diameter, Spherotech) or carboxylate modified polystyrene microparticles (0.9 μm diameter, Aldrich). The mixture was stirred for 1 h at room temperature, to induce particle swelling, followed by addition of a solution of **1EP** in cold THF (140 μL, 2.0 mM). After stirring for additional 1 h at 4 °C, the mixture was centrifuged at 7,000 rpm for 2 mins. The blue supernatant was discarded, and the blue pellet containing the stained microparticles was washed two times by adding 1 mL of aqueous sodium dodecylsulfate (0.05 % w/v) followed by centrifugation at 7,000

rpm. The particles were finally washed with water and resuspended in water (140 μL). *Hydrophobic silica surface:* A microsyringe was used to make spots from a stock solution of **1EP** (1.5 mM, $CDCl_3$) on a reverse-phase TLC plate (Analtech-Uniplate) that supported a 250 μm layer of porous silica gel particles (15 μm diameter) with impregnated C18 hydrocarbon.

Chemiluminescence and Fluorescence Imaging

Two sets of instrumentation were employed. *Xenogen IVIS® Lumina imaging system (Caliper Life Sciences, Alameda, CA, USA) with a thermoelectrically cooled CCD camera:* Solid phase and solution samples were placed on a heated stage set to 40 °C and a 5 cm field of view. Typically, the chemiluminescence was acquired over 60 s with 8 × 8 binning, no filter, and the lens aperture fully open (F_{stop}=1). Pixel intensity maps were acquired using Living Image software version 3.0, and the data was analyzed using ImageJ software version 1.43r. *Andor iXon EMCCD camera with a thermoelectrically cooled CCD and a 25 mm lens:* Solution samples were placed on a heated stage and chemiluminescent spectra were acquired using an Acton spectrometer with monochromator set to 750 nm and 1 mm slit width. Fluorescence spectra employed a laser (~200 μW) for excitation at 650 nm with 8 ms acquisition time.

Animal Imaging

Animal care and handling procedures were approved by the Notre Dame Institutional Advisory Committee of Animal Care. The nude mouse (strain NCr $Foxnl^{nu}$) in Fig. 3 was euthanized by cervical dislocation before study and the carcass maintained at 38 °C using a heating pad and heated stage. The carboxylate functionalized **1EP**-microparticles dispersed in water (50 μL, containing ~10^9 microparticles and 50 nmol of **1EP)** were injected subcutaneously. The chemiluminescence images were acquired for 5 mins with 8 × 8 binning. The fluorescence images were acquired for 1 sec with 4 × 4 binning. The live nude mouse in Fig. 4 was anesthetized using 2–3% v/v isoflurane and maintained at 1.5–2% v/v isoflurane during imaging. The tube containing **1EP** was maintained at 38 °C and the chemiluminescence images were acquired for 5 mins with 8 × 8 binning. The fluorescence images were acquired for 5 sec with 2 × 2 binning.

Acknowledgments

The authors are grateful to the National Science Foundation (grant no. CHE 0748761 to B.D.S.) and the University of Notre Dame Integrated Imaging Facility for financial support.

References

1. Mettler, FA.; Guiberteau, MJ. Essentials of Nuclear Medicine Imaging 5th Edition. New York: Saunders; 2005.
2. Mancini JG, Ferrandino MN. The impact of new methods of imaging on radiation dosage delivered to patients. Curr. Opin. Urol 2010;20:163–168. [PubMed: 19940771]
3. Sharkey RM, Goldenberg DM. Novel radioimmunopharmaceuticals for cancer imaging and therapy. Curr. Opin. Invest. Drugs 2008;9:1302–1316.
4. Roda, A., editor. Chemiluminescence and Bioluminescence: Past, Present and Future. Cambridge, UK: Royal Society; 2010.
5. Su Y, Chen H, Wang Z, Lv Y. Recent advances in chemiluminescence. Appl. Spectrosc. Rev 2007;42:139–176.
6. Prescher JA, Contag CH. Guided by the light: visualizing biomolecular processes in living animals with bioluminescence. Curr. Opin. Chem. Biol 2010;14:80–89. [PubMed: 19962933]
7. Roda A, Guardigli M, Michelini E, Mirasoli M. Bioluminescence in analytical chemistry and in vivo imaging. Trends Analyt. Chem 2009;28:307–322.

8. Gassensmith JJ, Baumes JM, Smith BD. Discovery and early development of squaraine rotaxanes. Chem. Commun 2009:6329–6338.
9. Adam W, Kazakov DV, Kazakov VP. Singlet-oxygen chemiluminescence in peroxide reactions. Chem. Rev 2005;105:3371–3387. [PubMed: 16159156]
10. Gassensmith JJ, et al. Synthesis and photophysical investigation of squaraine rotaxanes by “clicked capping”. Org. Lett 2008;10:3343–3346. [PubMed: 18582079]
11. Arunkumar E, Sudeep PK, Kamat PV, Noll BC, Smith BD. Singlet oxygen generation using iodinated squaraine and squaraine-rotaxane dyes. New J. Chem 2007;31:677–683.
12. Salice P, et al. Photophysics of squaraine dyes: role of charge-transfer in singlet oxygen production and removal. J. Phys. Chem. A 2010;114:2518–2525. [PubMed: 20121177]
13. Gassensmith JJ, Baumes JM, Eberhard J, Smith BD. Cycloaddition to an Anthracene Derived Macrocyclic Receptor with Supramolecular Control of Regioselectivity. Chem. Commun 2009:2517–2519.
14. Aubry JM, Pierlot C, Rigaudy J, Schmidt R. Reversible binding of oxygen to aromatic compounds. Acc. Chem. Res 2003;36:668–675. [PubMed: 12974650]
15. Bloodworth, AJ.; Eggelte, HJ. Singlet Oxygen. Frimer, AA., editor. Vol. Vol. 2. Boca Raton: CRC Press; 1985. p. 93-203.
16. Matsumoto M, Yamada M, Watanabe N. Reversible 1,4-cycloaddition of singlet oxygen to N-substituted 2-pyridones: 1,4-endoperoxide as a versatile chemical source of singlet oxygen. Chem. Commun 2005:483–485.
17. Descalzo AB, et al. Phenanthrene-fused boron-dipyrromethanes as bright long-wavelength fluorophores. Org. Lett 2008;10:1581–1584. [PubMed: 18355071]
18. So M–K, Xu C, Loening AM, Gambir SS, Rao J. Self-illuminating quantum dot conjugates for in vivo imaging. Nat Biotech 2006;24:339–343.
19. Frangioni JV. The problem is background, not signal. Mol. Imaging 2009;8:303–304. [PubMed: 20003888]
20. Branchini BR, et al. Red-emitting luciferases for bioluminescence reporter and imaging applications. Anal. Biochem 2010;396:290–297. [PubMed: 19748472]
21. Piatkevich KD, Verkhusha VV. Advances in engineering of fluorescent proteins and photoactivatible proteins with red emission. Curr. Opin. Chem. Biol 2010;14:23–29. [PubMed: 19914857]
22. Ma N, Marshall AF, Rao J. Near-infrared light emitting luciferase via biomineralization. J. Am. Cem. Soc. 2010 ASAP.
23. Troy T, Jekic-McCullen D, Sambucetti L, Rice B. Quantitative comparison of the sensitivity of detection of fluorescent and bioluminescent reporters in animal models. Mol. Imaging 2004;3:9–23. [PubMed: 15142408]
24. Tuchin, VV. Tissue Optics 2nd Ed.. Bellingham, Washington: SPIE Press; 2007.
25. Krasnovsky AA Jr. Luminescence and photochemical studies of singlet oxygen photonics. J. Photochem. Photobiol. A 2008;196:210–218.
26. Chapelon R, Balny C. Role of singlet oxygen in the thermal decomposition of the photooxide of l, 4-dimethoxy-9,10-dipyridylanthracene. Mol. Photochem 1971;3:255–259.
27. Fu Y, Krasnovsky AA Jr. Foote CS. Singlet oxygen dimol-sensitized luminescence from thermally generated singlet oxygen. J. Am. Chem. Soc 1993;115:10282–10285.
28. Kazakov DV, et al. Chemiluminescence during decomposition of 1,4-dimethylnaphthalene endoperoxide on the silica gel and alumina surface. Russ. Chem. Bull. Intl. Ed 2007;56:205–210.
29. Ishii H, Tsukino K, Sekine M, Nakata M. Singlet oxygen-sensitized delayed emissions from hydrogen peroxide/gallic acid/potassium ferricyanide systems containing organic solvents. Chem. Phys. Lett 2009;474:285–289.
30. Lin J-M, Liu M. Singlet oxygen generated from the decomposition of peroxymonocarbonate and its observation with chemiluminescence method. Spectrochim. Acta. A 2009;72:126–132.
31. Baigel DM, Gorman AA, Hamblett I, Hill TJ. Concerning the triplet energies of non-metallated phthalocyanines and the mechanism of singlet oxygen ($^1\Delta_g$)-sensitized phthalocyanine luminescence. J. Photochem. Photobiol. B 1998;43:229–231.

32. Murphy ST, Kondo K, Foote CS. Singlet-oxygen-sensitized delayed fluorescence: direct detection of triplet phthalocyanine as an intermediate. J. Am. Chem. Soc 1999;121:3751–3755.
33. Krasnovsky AA Jr. Litvin FF. Long-lived afterglow of photosynthetic pigments in solution: photochemiluminescence. Photochem. Photobiol 1974;20:133–149.
34. Hatz S, Poulsen L, Ogilby PR. Time-resolved singlet oxygen phosphorescence measurements from photosensitized experiments in single cells: effects of oxygen diffusion and oxygen concentration. Photochem. Photobiol 2008;81:1284–1290. [PubMed: 18435700]
35. Dysart JS, Singh G, Patterson MS. Calculation of singlet oxygen dose from photosensitizer fluorescence and photobleaching during mTHPC photodynamic therapy of MLL cells. Photochem. Photobiol 2005;81:196–205. [PubMed: 15469385]
36. Pellieux C, Dewilde A, Pierlot C, Aubry J-M. Bactericidal and virucidal activities of singlet oxygen generated by thermolysis of naphthalene endoperoxides. Method. Enzymol 2000;319:197–207.
37. Otsu K, et al. Impaired activation of caspase cascade during cell death induced by newly synthesized singlet oxygen generator, 1-buthylnaphthalene-4-propionate endoperoxide. Cell Biol. Int 2008;32:1380–1387. [PubMed: 18782624]
38. Agawa H, Nakazono M, Nanbu S, Zaitsu K. Chemiluminescence change of polyphenol dendrimers with different core molecules. Org. Lett 2008;10:5171–5174. [PubMed: 18954060]
39. Lee CC, Mackay JA, Fréchet JMJ, Szoka FC. Designing dendrimers for biological applications. Nat. Biotechnol 2005;23:1517–1526. [PubMed: 16333296]
40. Xiao S, Fu N, Peckham K, Smith BD. Efficient synthesis of fluorescent squaraine rotaxane dendrimers. Org. Lett 2010;12:140–143. [PubMed: 19957971]
41. Ullman EF, et al. Luminescent oxygen channeling immunoassay: measurement of particle binding kinetics by chemiluminescence. Proc. Natl. Acad. Sci. USA 1994;91:5426–5430. [PubMed: 8202502]
42. Cao Y, Koo Y-EL, Koo SM, Kopelman R. Ratiometric singlet oxygen nano-optodes and their use for monitoring photodynamic therapy nanoplaforms. Photochem. Photobiol 2005;81:1489–1498. [PubMed: 16107183]
43. Borisov SM, Klimant I. Luminescent nanobeads for optical sensing and imaging of dissolved oxygen. Microchim. Acta 2009;164:7–15.
44. Chen J, Zeng F, Wu SZ, Chen QM, Tong Z. A core-shell nanoparticle approach to photoreversible fluorescence modulation of a hydrophobic dye in aqueous media. Chem. Eur. J 2008;14:4851–4860.
45. Linet MS, Kim KP, Rajaraman P. Children's exposure to diagnostic medical radiation and cancer risk: epidemiologic and dosimetric considerations. Pediatr. Radiol 2009;39 supp 1:S4–S26. [PubMed: 19083224]
46. Stoddart JF. The chemistry of the mechanical bond. Chem. Soc. Rev 2009;38:1802–1820. [PubMed: 19587969]
47. Kay ER, Leigh DA, Zerbetto F. Synthetic molecular motors and mechanical machines. Angew. Chem. Int. Ed 2007;46:72–191.

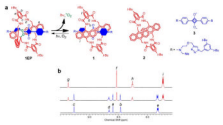

Figure 1. Thermal cycloreversion of 1EP to 1 and reverse photoreaction

a, Cycloreversion of **1EP** releases singlet oxygen and emits near-infrared light. The encapsulated blue component in rotaxane **1** and **1EP** is the squaraine **3. b**, Partial ^{1}H NMR spectra ($CDCl_3$) showing photoconversion of **1** into **1EP:** (top) **1**, (middle) mixture of **1** and **1EP** after irradiation with red light for 10 mins, (bottom) complete conversion to **1EP** after irradiation for 30 mins.

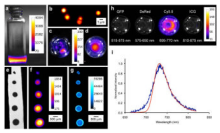

Figure 2. False-colored pixel intensity maps at 38 °C with intensity scales in arbitrary units

a, Vial containing a solution of chemiluminescent **1EP** in $CDCl_3$. **b**, Fluorescence micrograph of carboxylate functionalized polystyrene **1EP**-microparticles (0.9 μm diameter), **c**, Chemiluminescence from polystyrene **1EP**-microparticles that are aggregated in a vial of water (viewed from top), **d**, Chemiluminescence from carboxylate functionalized polystyrene **1EP**-microparticles that are dispersed throughout a vial of water, **e**, **f**, **g**, Bright field, chemiluminescence, and fluorescence images, respectively, of a reverse-phase TLC plate with spots of **1EP**. **h**, Chemiluminescence from a solution of **1EP** viewed with different emission filters, **i**, Chemiluminescence (blue) and fluorescence (red, excitation = 650 nm) emission spectra of **1EP** (1.5 mM, $C_2D_2C1_4$) at 65 °C.

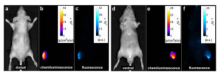

Figure 3. Chemiluminescence and reflected fluorescence from 1EP-microparticles injected subcutaneously into the dorsal side of a nude mouse rear leg at 38 °C

a, **b**, **c**, Dorsal bright field, chemiluminescence, and fluorescence images (chemiluminescence and fluorescence TBR = 6.9 and 29, respectively). **d**, **e**, **f**, Ventral images which required light penetration through deeper tissue (chemiluminescence and fluorescence TBR = 6.8 and 4.4, respectively). N = 2

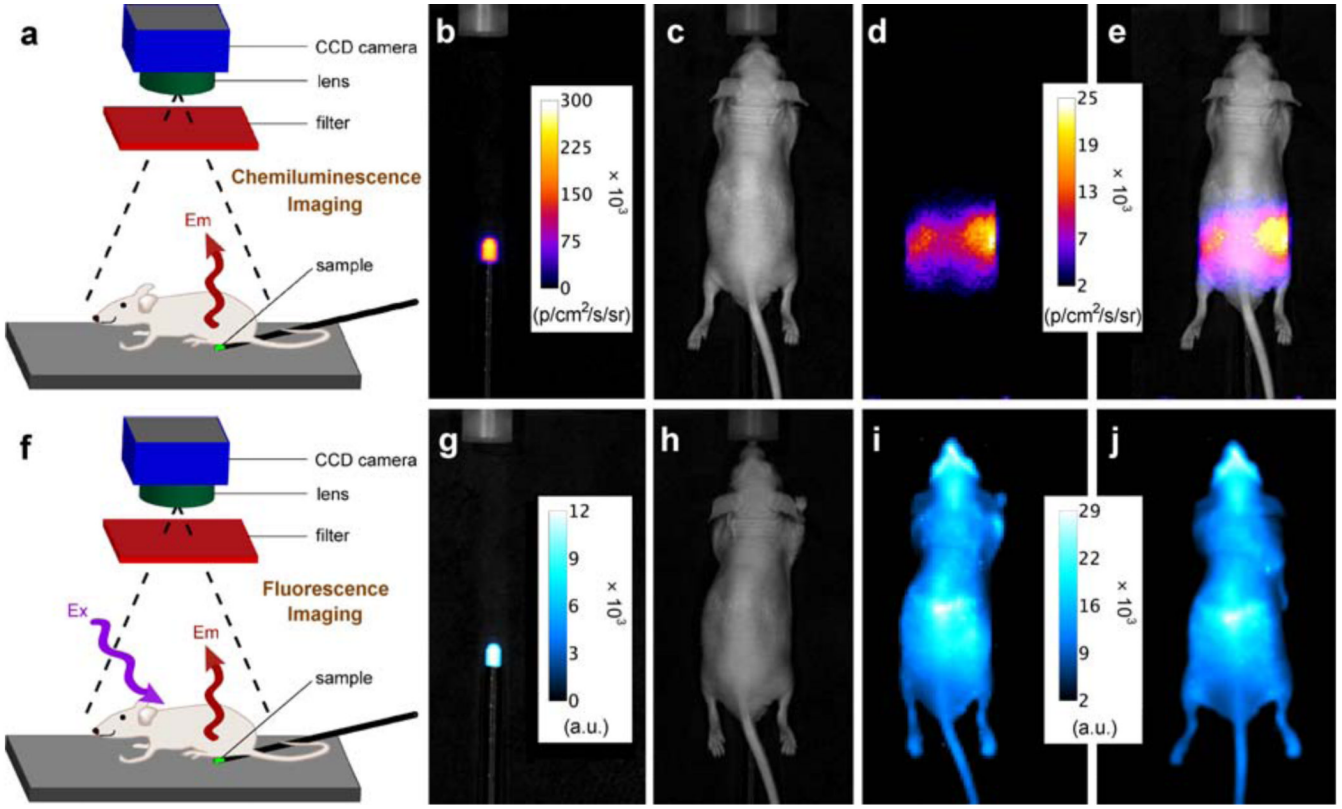

Figure 4. Chemiluminescence from 1EP at 38 °C penetrates through a living nude mouse

a, **f**, Experimental set-up for chemiluminescence and fluorescence imaging, respectively. **b**, **g**, Chemiluminescence and fluorescence pixel intensities from a small tube containing **1EP** (250 nmol) in $C_2D_2Cl_4$. **c**, **h**, Photograph of mouse located above the tube. **d**, **e**, Pixel intensity map of chemiluminescence that is transmitted through the mouse (TBR = 11.6). **i**, Fluorescence intensity map of mouse located above the tube (TBR = 1.1). **j**, Fluorescence intensity map of mouse with no tube present.